Quantitative time domain analysis of lifetime-based Förster resonant energy transfer measurements with fluorescent proteins: Static random isotropic fluorophore orientation distributions

Alexandrov, Yuriy; Nikolic, Dino Solar; Dunsby, Christopher; French, Paul M.W.

Published in:
Journal of Biophotonics

Link to article, DOI:
10.1002/jbio.201700366

Publication date:
2018

Document Version
Publisher's PDF, also known as Version of record

Received: 6 December 2017 | Accepted: 23 March 2018

DOI: 10.1002/jbio.201700366

Journal of BIOPHOTONICS

FULL ARTICLE

Quantitative time domain analysis of lifetime-based Förster resonant energy transfer measurements with fluorescent proteins: Static random isotropic fluorophore orientation distributions

Yuriy Alexandrov[1,2*] | Dino S. Nikolic[3] | Christopher Dunsby[1,2,4] | Paul M. W. French[1,2]

[1]Photonics Group, Department of Physics, Imperial College London, London, UK

[2]Light Microscopy, Francis Crick Institute, London, UK

[3]Quantum Physics and Information Technology Group, Technical University of Denmark, Kgs. Lyngby, Denmark

[4]Centre for Pathology, Imperial College London, London, UK

***Correspondence**
Yuriy Alexandrov, Photonics Group, Department of Physics, Imperial College London, Prince Consort Road, London SW7 2AZ, UK.
Email: yuriy.alexandrov@imperial.ac.uk

Funding information
Biotechnology and Biological Sciences Research Council, Grant/Award Number: BB/M006786/1; Medical Research Council, Grant/Award Number: MR/K015834/1

Förster resonant energy transfer (FRET) measurements are widely used to obtain information about molecular interactions and conformations through the dependence of FRET efficiency on the proximity of donor and acceptor fluorophores. Fluorescence lifetime measurements can provide quantitative analysis of FRET efficiency and interacting population fraction. Many FRET experiments exploit the highly specific labelling of genetically expressed fluorescent proteins, applicable in live cells and organisms. Unfortunately, the typical assumption of fast randomization of fluorophore orientations in the analysis of fluorescence lifetime-based FRET readouts is not valid for fluorescent proteins due to their slow rotational mobility compared to their upper state lifetime. Here, previous analysis of effectively static isotropic distributions of fluorophore dipoles on FRET measurements is incorporated into new software for fitting donor emission decay profiles. Calculated FRET parameters, including molar population fractions, are compared for the analysis of simulated and experimental FRET data under the assumption of static and dynamic fluorophores and the intermediate regimes between fully dynamic and static fluorophores, and mixtures within FRET pairs, is explored. Finally, a method to correct the artefact resulting from fitting the emission from static FRET pairs with isotropic angular distributions to the (incorrect) typically assumed dynamic FRET decay model is presented.

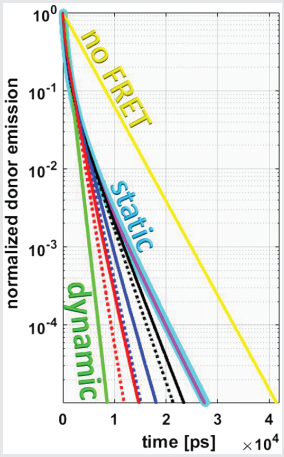

KEYWORDS

biosensors, fluorescence, fluorescent proteins, Förster resonant energy transfer (FRET), molecular dynamics, protein-protein interactions

1 | INTRODUCTION

Förster resonant energy transfer (FRET) [1] is the non-radiative transfer of energy from an excited donor fluorophore to a proximate acceptor fluorophore (or fluorophores) through the short-range dipole-dipole interaction that results in relaxation of the excited singlet state of the former and the promotion to the excited singlet state of the latter. Measurements of fluorescence in spectrofluorometers or imaging systems are widely used for FRET-based

Chris Dunsby and Paul M. W. French contributed equally to this study.

analysis of molecular interactions or changes in conformation of biosensors. Such molecular dynamics can be quantified through calculations of FRET efficiency and/or the FRETing population fraction. Detecting and/or quantifying biomolecular processes using FRET-based readouts is important for basic research and drug discovery, including for assays of protein-protein interactions.

The FRET rate, $k_{FRET,}$ depends on the spectral overlap of the donor emission and acceptor excitation spectra, on the relative orientation of their excitation/emission dipoles, and scales inversely with a sixth power dependence on the distance, R_{DA}, between donor and acceptor fluorophore dipoles [2]:

$$k_{FRET} = \frac{1}{\tau_D}\left(\frac{R_{DA}}{R_f}\right)^{-6} = \frac{1}{\tau_D}\frac{3}{2}\eta^{-6}\kappa^2, \quad (1)$$

where τ_D is the donor fluorescence lifetime in the absence of FRET and R_f is the "Förster distance" given by [3]:

$$R_f = 0.02108\sqrt[6]{\kappa^2 n^{-4} Q_D J}(\text{nm}). \quad (2)$$

In Eq. (2), κ^2 is the orientation factor for dipole-dipole coupling, n is the refractive index of the medium, Q_D is the fluorescence quantum yield of the donor fluorophore in the absence of the acceptor and J is the overlap integral of the donor emission and acceptor excitation spectra. It is widely assumed that the FRETing fluorophores are highly mobile during their fluorescence decay, such that their relative dipole orientations present a random distribution over the decay time, and so the time-averaged value of κ^2 is 2/3 for each FRET pair [2].

As the dependence of the FRET rate on κ^2 is central for the work presented here, we will further use the dimensionless donor-acceptor distance parameter $\eta = R_{DA}/R_0$ as specified in Eq. (1) to emphasize the direct proportionality of the FRET rate to the orientation factor κ^2. Here, the distance R_0 is the Förster distance, R_f, calculated for $\kappa^2 = 2/3$. We note that Eq. (1) is only applicable to cases where the orientation factor κ^2 is constant during the decay: this assumption will be discussed further below. If we assume that the unquenched donors' fluorescence decay profile is monoexponential, a constant k_{FRET} will therefore result in the donor fluorophore exhibiting a monoexponential fluorescence decay in the presence of FRET. Another important characteristic of FRET that we will investigate is the FRET efficiency, which is defined as the proportion of excitation events resulting in FRET, that is, $E = \frac{k_{FRET}}{k_D + k_{FRET}}$, where $k_D = 1/\tau_D$ is the decay rate of the donor in the absence of FRET.

For most commonly used fluorophores—including fluorescent proteins—the R_f and R_0 distances are on the order of a few nm and this effectively means that FRET is only significant for fluorophores separated by less than ~10 nm. This high sensitivity to fluorophore proximity has led to FRET being widely used in biological studies to detect interactions between fluorescently labelled molecules or moieties [4], or to read out cleaving or changes in conformation of FRET constructs that are labelled with both donor and acceptor fluorophores [5]. Quantitative FRET measurements can provide information about the donor-acceptor distance and the fraction of a population of donor fluorophores undergoing FRET. Thus FRET-based imaging techniques can be used to map and quantitate molecular interactions in space and time. The use of FRET with genetically expressed fluorescent proteins as labels is useful to elucidate signalling processes, such as protein binding or oligomerization, in cells. Furthermore, FRET can be used to provide dynamic readouts of biological function in live cells using genetically expressed fluorescent protein-based biosensors [6] that have been developed to report variations in concentrations of cell-signalling molecules including inositol 1,4,5-trisphosphate (IP3) [7], phosphatidylinositol (4,5)-bisphosphate (PIP2) [8] and calpain [9] or ions [10] such as calcium [11, 12], potassium [13] and chloride [14].

FRET can be detected and quantified through analysis of the change in donor and/or acceptor fluorescence via a range of different measurement techniques [15, 16]. Of these, the most commonly implemented are spectral ratiometric measurements of the ratio of sensitized acceptor to donor intensities, polarization-resolved measurements of fluorescence anisotropy and fluorescence lifetime measurements of the donor emission—noting that FRET provides an additional relaxation channel for excited donor fluorophores such that the fluorescence lifetime of the FRETing donors is reduced relative to the non-interacting donor's lifetime. Ratiometric measurements of donor and acceptor fluorescence intensity or anisotropy can be compromised by cross-talk between spectral (or polarization) channels and require measurements of reference samples [17] to provide quantitative measurements of FRET efficiency or FRETing population fraction [18]. However, fluorescence lifetime measurements of FRET require only the donor emission to be detected and analysed in a single spectral channel, avoiding artefacts due to cross-talk, and fluorescence lifetime measurements are independent of the spectral attenuation profile of the instrument or sample. Furthermore, in the case of a donor fluorophore with a monoexponential decay with lifetime τ_D and a constant FRET rate, the FRETing donor also exhibits a monoexponential decay, with lifetime $\tau_{DA} = \frac{1}{k_D + k_{FRET}} = \tau_D(1-E)$, and both τ_{DA} and the fraction of FRETing donors, β_{DA}, can be determined by fitting the donor emission decay profile to a double exponential decay model [19, 20]:

$$I = I_0\left(\beta_{DA}e^{-t/\tau_{DA}} + (1-\beta_{DA})e^{-t/\tau_D}\right). \quad (3)$$

To map spatial variations of FRET, the fluorescence decay profiles can be analysed in each pixel to produce a map of fluorescence lifetime parameters and so fluorescence lifetime imaging (FLIM) can provide maps of FRET parameters, which can be interpreted as maps of molecular interactions or biosensor readouts. FLIM can also be applied with other biosensors or bioswitches that utilize quenching of fluorescence, for example, to map variations in chemical environment such as pH [21].

One drawback of fitting fluorescence decay data to double exponential or more complex models is that they require

significantly more detected photons to achieve a given accuracy than spectral or polarization ratiometric methods. Typically, a few hundred photons are required to fit a monoexponential decay profile to determine the fluorescence lifetime with 10% accuracy and >10 000 photons are required to fit more complex decay profiles [22]. FLIM with 1000s of photons detected per pixel would typically result in significant photobleaching (which can compromise lifetime and FRET measurements) and phototoxicity (which could compromise measurements of dynamic events in live cells). For many (indeed most) applications, including extended live cell imaging and "high throughput" automated multiwell plate FLIM, it is desirable to make measurements requiring only a few hundred photons per pixel to be detected. To this end, it is therefore common to fit complex fluorescence decay profiles to a monoexponential decay model in order to provide empirical lifetime contrast, including for FRET experiments, or to use phasor analysis [23, 24]. If quantitative analysis of complex decay profiles is required, a "global binning" approach can be employed. Here, photons detected across many pixels in a field of view (FOV) or region of interest (ROI) can be combined to provide the 1000s of photons required to fit to complex decay models. This will return a single set of lifetime values over the FOV or ROI. Individual pixel data can then be refitted with the lifetime parameters fixed to these globally determined values and only the pre-exponential factors allowed to vary, for example, to map the spatial variation of β_{DA}. Alternatively, all the pixels in a FOV or ROI can be analysed in parallel, fitting all the pixel data simultaneously to a complex decay model for which the lifetime values are assumed to be spatially invariant. We describe this latter approach, which is more robust [25] than global binning, as "global fitting." Such global analyses (ie, global binning or global fitting) can be extended across multiple FOV, for example, in a time series or a multiwell plate sample array [26–28].

To analyse such FLIM data, we have developed an open source software package called *FLIMfit* [29] that provides a post-acquisition pixelwise fitting and also global binning and global fitting capabilities. The latter utilizes a variable projection approach [30, 31] to provide global fitting of large FLIM data arrays (~100s FOV, consisting of 10^7-10^8 pixels) to double exponential models in minutes for FRET analysis. In principle, FLIM FRET determination of the FRETing population fraction, β_{DA}, can be combined with quantitative measurements of donor and acceptor concentrations (accessed via calibrated measurements of fluorescence intensity) to yield intracellular dissociation constants (K_D) of specific molecular interactions. Implemented in an automated multiwell plate instrument [28], such measurements could be used to map cell-signalling networks, for example, to screen with multiplexed FRET readouts, to assay off-target effects and to study combination therapies. The ability of automated multiwell plate FLIM FRET to provide single cell measurements from 1000s of cells in a single experiment offers the potential to study the heterogeneity in the response of a cell population, for example, to a drug candidate or genetic manipulation.

The utilization of FRET-based assays with genetically expressed fluorescent proteins is widespread and the interest in quantitative FRET-based assays, including using FLIM, is increasing. Quantitative analysis of FRET—for example, to obtain the FRET efficiency E and/or the FRETing population fraction β_{DA}—usually assumes a homogeneous population of FRETing fluorophore pairs with constant FRET efficiency (ie, constant R_{DA} and J) and highly dynamic, randomly orientated fluorophores such that the dipole orientation factor of the donor and acceptor averages to $\kappa^2 = 2/3$ on a timescale much shorter than τ_D. These assumptions should lead to the FRETing donor exhibiting a monoexponential decay profile (assuming a monoexponential decay profile for the non-FRETing donor).

However, as eloquently explained using Monte Carlo simulations by Vogel et al. in [3], if there is heterogeneity in the donor-acceptor separation, spectral overlap or dipole orientation factor, this heterogeneity can result in complex (multipeaked) distributions of FRET efficiency and complex fluorescence decay profiles for FRETing donor fluorophores conventionally expected to present monoexponential decay profiles. This can lead to errors in the estimation of the FRET efficiency, the donor-acceptor separation and the FRETing population fraction. Vogel et al. also explained that bimodal FRET efficiency distributions can result from acceptor dark states, for example, [32, 33], but Vogel et al. argued that this was unlikely, at least in the case of the "C5V" Cerulean-Venus FRET constructs, and instead attributed it to the lack of dynamic averaging of the fluorophore dipole orientations during the fluorescence decay time of the donor.

The size of fluorescent proteins means that they are effectively static on the timescale of their fluorescence decay (<~5 nanosecond), since their rotational correlation time is typically much longer (>~15 nanosecond). This means that the assumption $\kappa^2 = 2/3$—based on a population of independent, dynamic fluorophores with rapidly evolving, random dipole orientations drawn from isotropic distributions—is not valid. Vogel et al. postulated that a static isotropic distribution of donor and acceptor fluorophore orientations would be a more physically realistic model and, following previous work, for example, [34–38], showed that this can also result in complex (bimodal) distributions of κ^2 and therefore of FRET efficiency, with corresponding complexity manifest in the fluorescence decay profiles—even with constant R_{DA} and J. Clearly, this could compromise quantitative FRET measurements of donor-acceptor distance or FRETing population fraction when utilizing fluorescent protein labels. In [3], the authors presented an analytic model for the distribution of FRET efficiencies, $p_{FRET\ s\kappa 2}(E)$, for a population of

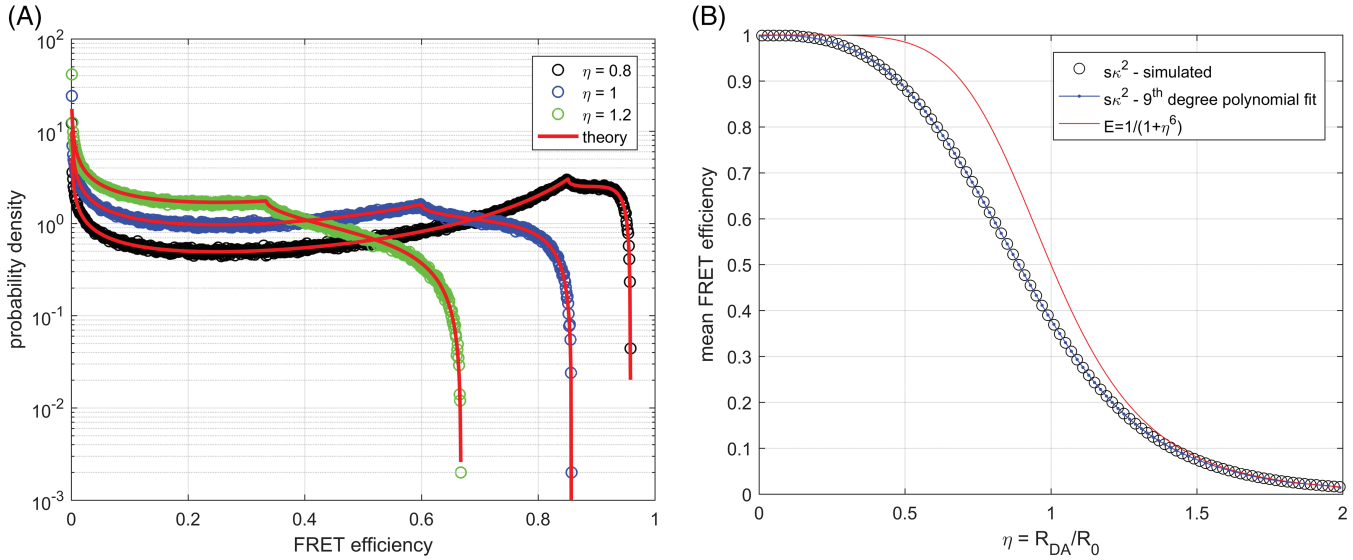

FIGURE 1 A, Plots of $p_{\mathrm{FRET}\ s\kappa 2}(E)$ as a function of E for $\eta = [0.8, 1.0, 1.2]$. Points show results of numerical simulations and curves show the analytical model from [3]. B, Plot of the mean FRET efficiency as a function of η for the $s\kappa^2$ model (black open circles) and the $d\kappa^2$ model (solid red line). The blue line shows a polynomial approximation of the $\langle E\rangle(\eta)$ dependence of the $s\kappa^2$ model that is subsequently used to calculate the mean FRET efficiency from values of η returned from the fitting

FRET pairs in the "static isotropic regime" and, in a subsequent paper [39], provided a formula for correcting experimentally determined donor-acceptor distances originally calculated using the standard assumption of $\kappa^2 = 2/3$ and fitting the donor decay to a double exponential decay model. This approach agreed well with estimates based on a previously published approximation [40] to the effective ensemble average dipole orientation factor $\langle\kappa^2\rangle = \frac{2}{3}(1-\langle E\rangle)$ for the static random isotropic dipole orientation regime.

In this article, we aim to analyse the impact of the slow rotational decorrelation of fluorescent proteins compared to their fluorescence lifetimes on quantitative FRET assays, particularly, assays of the FRETing population fractions and K_{D}s.

2 | OVERVIEW OF METHODOLOGY AND ANALYSIS

As discussed in Section 4, we used numerical simulation to generate the "experimental" fluorescence decay profiles expected for static, isotropically orientated FRETing fluorophores (which we refer to as the "$s\kappa^2$" model). We demonstrate that our $s\kappa^2$ simulation of the probability distribution of FRET efficiencies for 3 different values of η agrees well (Figure 1A) with the analytic solution from [3] and we show (Figure 1B) how the mean FRET efficiency varies as a function of η for the simulated $s\kappa^2$ distribution compared with the theoretical curve for dynamic, randomly orientated donor-acceptor pairs (where the fluorophore rotational correlation times are much shorter than the fluorescence lifetime and which we refer to as the $d\kappa^2$ model of dipole orientation).

We then explore the potential impact of the $s\kappa^2$ decay model on experimental FRET measurements by generating a series of simulated $s\kappa^2$ fluorescence decays for different values of molar fraction of the FRETing donor, β_{DA}, for a range of donor-acceptor distances η. We analyse these simulated $s\kappa^2$ fluorescence decay profiles with a nonlinear least-squares fitting MATLAB program (discussed in Section 4) that is able to fit fluorescence decay profiles to either the $d\kappa^2$ or $s\kappa^2$ models and to apply global fitting across multiple decay profiles. This capability is currently restricted to the analysis of one or a few fluorescence decay profiles and so is not yet able to be applied to FLIM data. We present exemplar simulated $s\kappa^2$ decay profiles and the results of fitting to each model (Figure 2) and illustrate how the FRET parameters obtained when fitting these simulated decay profiles to the $s\kappa^2$ or $d\kappa^2$ models would be expected to vary as a function of molar fraction of FRETing donor and for a range of donor-acceptor distances (Figure 3). This comparison was made for both local or global fitting and for different numbers of detected photons. By comparing the fit results with the corresponding values for donor lifetime τ_{D}, molar fraction β_{DA} and η used in the simulation, we confirm the practical applicability of fitting to the $s\kappa^2$ model. We also illustrate the errors that can result from applying an analysis based on the $d\kappa^2$ model to simulated $s\kappa^2$ decay profiles.

We then use Monte Carlo simulations of rotational diffusion to explore the transition between the $s\kappa^2$ model and the dynamic $d\kappa^2$ model, illustrating how this would be manifest in the resulting fluorescence decay profiles (Figure 4). These results support the use of the $s\kappa^2$ model for analysis of fluorescence lifetime data from FRET measurements with static random isotropically oriented fluorophores. The Monte Carlo simulations are shown to agree well (Figures 4 and 5)

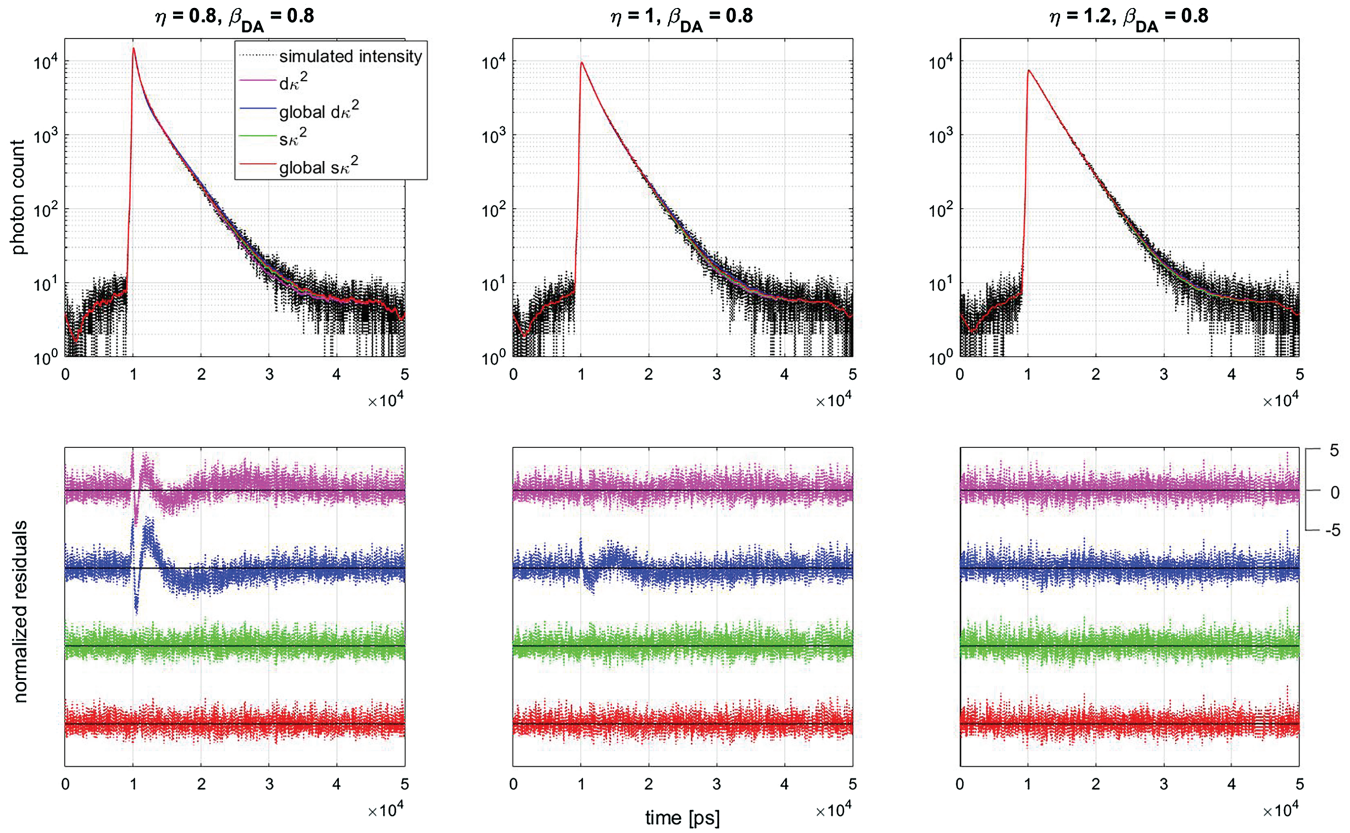

FIGURE 2 Exemplar fits to simulated $s\kappa^2$ decays using a range of different decay models. In the simulated decays $\beta_{DA} = 0.8$ and $N_{ph} = 2 \times 10^6$. Left, $\eta = 0.8$; centre, $\eta = 1$; right, $\eta = 1.2$. The top panels show the simulated decay together with the corresponding fits obtained using different fit models. The bottom panels show the normalized residuals for each fit model, all presented with the same scale and the corresponding zero levels shown by the horizontal black lines

with the analytic $s\kappa^2$ model of Eq. (15) and are also used to illustrate how the shape of the probability distribution for the FRET rate at a given time depends on the ratio of the fluorescence lifetime to the fluorophore rotational correlation time (Figure 6).

The final section explores the impact of fitting real experimental FLIM FRET data to $s\kappa^2$ or $d\kappa^2$ models, using data from FRET assays of protein interactions where the aim was to calculate K_D. Because we are not able to fit FLIM data to the $s\kappa^2$ model, we introduce a new approach enabling FRET parameters obtained from a $d\kappa^2$ fit of fluorescent protein FLIM data to be "corrected" to those expected for a $s\kappa^2$ fluorescence decay. We show the numerical validation of this approach (Figure 7) and discuss its application to experimental FLIM FRET data of Ras association domain family (RASSF)-mammalian sterile 20-like kinases (MST) interactions in Cos 7 cells (summarized in Tables 1 and 2). Finally, since one motivation of this work was to improve the determination of the K_D of protein interactions using lifetime-based FRET assays, we also explore the impact of dark acceptor states on quantitative FRET readouts and show (Figure 8A) that, at least for the RASSF-MST interactions considered here, their impact on the calculated K_D values is likely to be less than that of the incorrect analysis of $s\kappa^2$ fluorescence decay profiles using a $d\kappa^2$ fitting model.

3 | RESULTS AND DISCUSSION

3.1 | Impact of static random isotropic distribution of FRET dipole orientations

We used the analytic model of Vogel et al. [3] to generate $s\kappa^2$ probability distribution of FRET efficiencies for values of η ranging from 0 to 2 and compared these distributions with numerical simulations using Eq. (15), as discussed in Section 4. These curves are shown in Figure 1A. We also compared the mean FRET efficiency as a function of η for both the $s\kappa^2$ and $d\kappa^2$ models of dipole orientation with the same FRET parameters, see Figure 1B. These FRET efficiency curves can be seen to differ, particularly in the range $0.3 < \eta < 1.2$.

We then simulated the $s\kappa^2$ donor population fluorescence decay profiles for a range of 17 FRETing donor molar fractions, β_{DA}, from 0.1 to 0.9, in steps of 0.05, with the non-FRETing donor lifetime fixed at 3500 picosecond and FRET efficiencies corresponding to 3 values of $\eta = [0.8, 1.0, 1.2]$. These fluorescence decay profiles were calculated for a total number of photons in the decay of $N_{ph} = 2 \times 10^6$ and 10^8. The simulated decay profiles were fitted to the $d\kappa^2$ model with N_{ph}, β_D, τ_D, τ_{DA} as fitting parameters, and to the analytic $s\kappa^2$ model of [3] with N_{ph}, β_D, τ_D, η as fitting parameters, as discussed in Section 4. Fitting was applied locally (ie, on a per fluorescence decay profile basis) for each of the

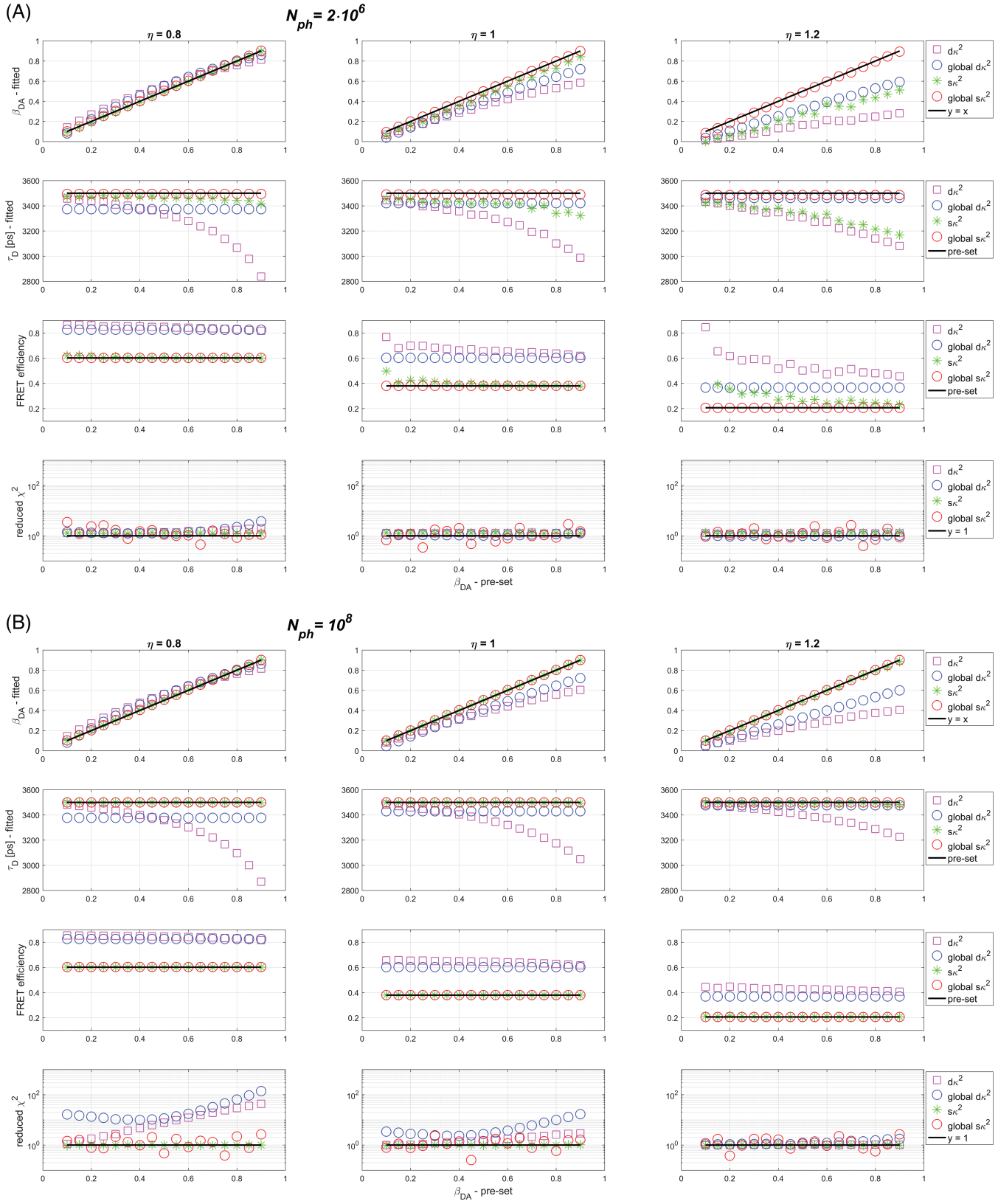

FIGURE 3 Recovered fit parameters as a function of the preset FRETing donor molar fraction β_{DA} for different approaches to fit simulated $s\kappa^2$ data. Plots are grouped in 3 columns according to the preset values of donor-acceptor distance parameter η of the $s\kappa^2$ simulation (η = [0.8, 1.0, 1.2]). The last row of plots shows the behaviour of the fitting error χ^2. To examine sensitivity of fitting to S/N, the decays were simulated for the total numbers of photons in the decay of (A) $N_{ph} = 2 \times 10^6$ and (B) $N_{ph} = 10^8$

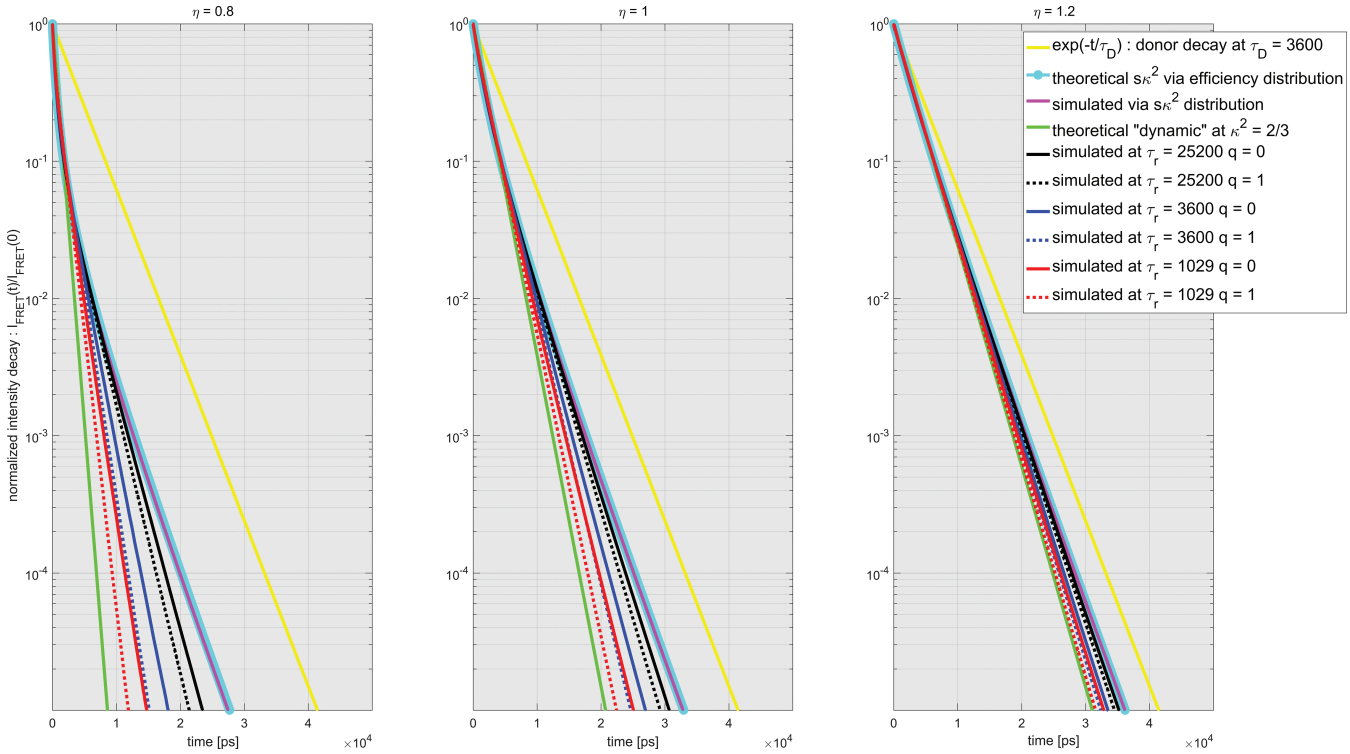

FIGURE 4 Theoretical normalized FRET intensity decays for $\tau_D = 3600$ picosecond and simulated decay curves for different rotational correlation times of the donor and acceptor. Here, the decay curve was not convolved with an IRF. Separate plots are shown for increasing values of η (left to right). For the simulated decay curves, solid lines represent $q = 0$ (static donor or acceptor) and dashed lines represent q = 1 (equal rotational correlation time of donor and acceptor)

17 donor molar fractions and globally. For the global analysis, 2 global nonlinear parameters (τ_D, τ_{DA}) were fitted when using the double exponential ($d\kappa^2$) model and 2 global nonlinear parameters (τ_D, η) were fitted when using the $s\kappa^2$ model. The linear amplitudes for the FRETing and non-FRETing components were determined on a per-decay basis. Exemplar simulated decays together with fits using the different decay models are shown in Figure 2 for three specific cases.

Figure 3 shows the values of β_{DA}, τ_D, and <E>, and obtained using the various fitting approaches and how they vary as a function of the simulated β_{DA} values. The last row of plots shows the corresponding variation in the χ^2 goodness-of-fit parameter. These plots are given for 3 different values of η and for 2 different values of N_{ph}. It is clear that the fit to the conventional double exponential decay profile consistently overestimates the FRET efficiency, underestimates τ_D and, in general, underestimates β_{DA} of the underlying $s\kappa^2$ model.

A further observation is that the accuracy of fitting to the $s\kappa^2$ model is significantly improved by the global fitting method. We attribute this to the effective reduction in the number of parameters fitted per decay.

In order to check for a possible dependence of these results on the value of τ_D, the simulations were repeated at several settings starting from $\tau_D = 1200$ picosecond and up to $\tau_D = 6500$ picosecond. The results were similar to those presented in Figures 2 and 3 and it was concluded that there is no significant dependence on τ_D.

3.2 | Applicability of static and dynamic models of (isotropic) fluorophore dipole orientations

Although we believe the $s\kappa^2$ model is a reasonable approximation of the fluorescent protein donor emission, the dynamics of any real FRETing donor fluorophores will lie

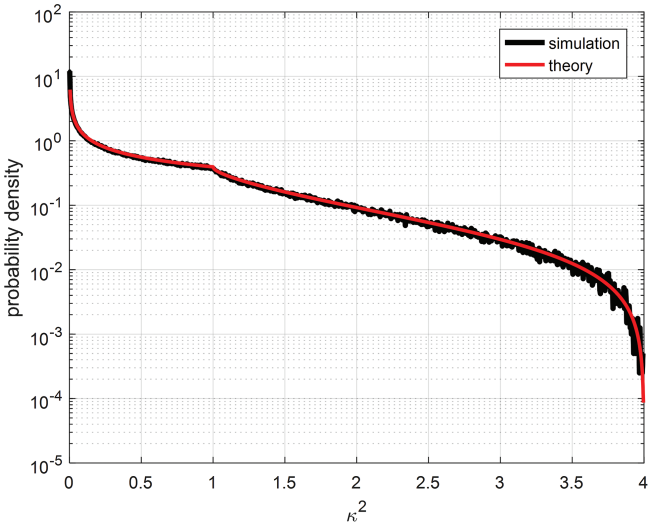

FIGURE 5 Theoretical and simulated PDDFs of the static random isotropic orientation factor κ^2. The theoretical curve was obtained from Eq. (20). The simulated curve is obtained through Monte Carlo simulation of randomly oriented donor-acceptor pairs. The average of this distribution is 2/3 [41]

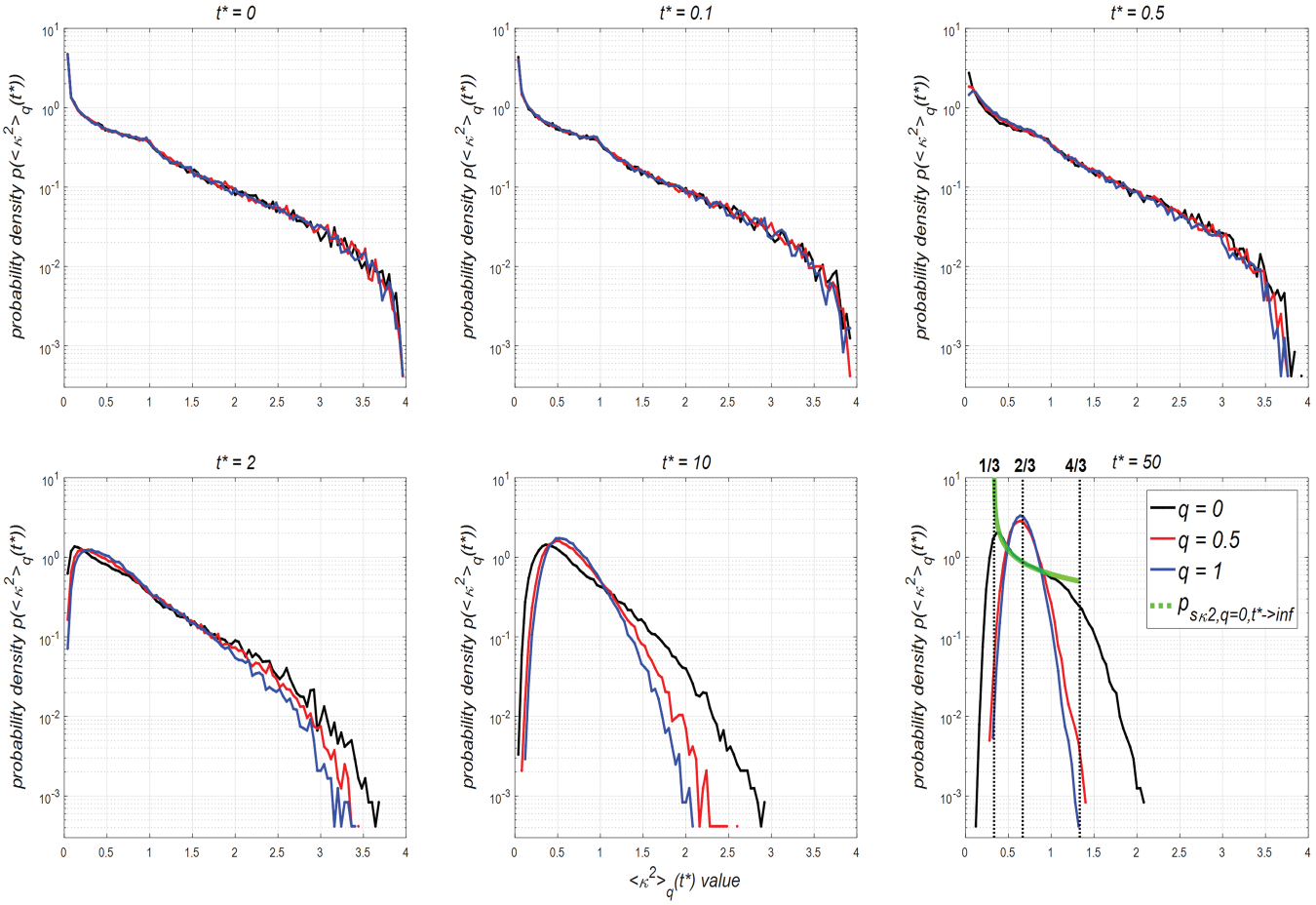

FIGURE 6 Plots of the distributions of the variable $<\kappa^2>_q(t^*)$ for different times t^*. Sixty thousand realizations of $\kappa^2_q(t^*)$ were used to generate each PDDF. Each realization consisted of 1645 time steps. For the $t^* = 50$ plot (which is closest to the dynamic limit $t^* \rightarrow \infty$), the analytical function $p_{s\kappa 2,q=0,t^*\rightarrow\infty}(\kappa^2) = 1/\left(2\sqrt{\kappa^2 - 1/3}\right)$ is shown over the range $<\kappa^2>_q(t^*) = 1/3 \ldots 4/3$ to illustrate the $<\kappa^2>_q(t^*)$ PDDF for $q = 0$ in the limit $t^* \rightarrow \infty$ and a dashed vertical line at $<\kappa^2>_q(t^*) = 2/3$ is shown to illustrate the limit as $t^* \rightarrow \infty$ for the case $q = 1$

somewhere between the $s\kappa^2$ and the $d\kappa^2$ models. The amount of rotational motion that occurs during the fluorescence decay will depend on the ratio of the fluorescence decay time to the fluorophore rotational correlation time. To explore the applicability of the $s\kappa^2$ model to real-life fluorescent protein-based FRET pairs and to inform the design of new FRET constructs, we carried out rotational diffusion-based simulations of FRET intensity decays (as described in Section 4) for donor and acceptor fluorophores with different rotational correlation times, τ_{rD} and τ_{rA}, and explored the impact of using dissimilar donor and acceptor fluorophores—as could be envisaged for FRET between a fluorescent protein and a dye. For this, we define $q = \min(\tau_{rD}, \tau_{rA})/\max(\tau_{rD}, \tau_{rA})$, that is, the ratio of the shorter to longer donor/acceptor rotational correlation time, and $\tau_r = \min(\tau_{rD}, \tau_{rA})$, the minimal rotational correlation time.

Figure 4 presents simulated donor fluorescence decay profiles based on rotational diffusion-based simulations for different rotational correlation times, τ_r, together with theoretical decay profiles calculated for the $s\kappa^2$ and $d\kappa^2$ models. The overall tendency is that donor fluorophores with rotational correlation times much greater than their fluorescence lifetimes, that is, $\tau_r >> \tau_D$ (black line) present fluorescence decay profiles that are closer to the $s\kappa^2$ limit (cyan and magenta curves), whereas the decay profiles of FRETing donor fluorophores with shorter rotational correlation times, that is, $\tau_r << \tau_D$ (red lines) are closer to the monoexponential decay profile of the dynamic averaging $d\kappa^2$ limit (green line). In Figure 4, the magenta curve represents the $s\kappa^2$ intensity decays simulated using Eq. (19) (see Section 4) for the case $\tau_{rD}, \tau_{rA} \rightarrow \infty$. The cyan curve represents the $s\kappa^2$ intensity decay profile calculated using Eq. (15) with the $p_{\text{FRET } s\kappa 2}(E)$ distribution taken from the analytical expression for the FRET efficiency distribution reported by Vogel et al. [3].

A theoretical model of the $s\kappa^2$ decay profile can also be obtained from Eq. (18) using a previously published analytical expression for the $s\kappa^2$ distribution [41] (the relevant equation is presented in Section 4 as Eq. (20)). The resulting decay is practically indistinguishable from the simulated (magenta) decay profile and so it is not shown in Figure 4. The excellent agreement between the analytic description of the κ^2 probability density distribution function (PDDF) given

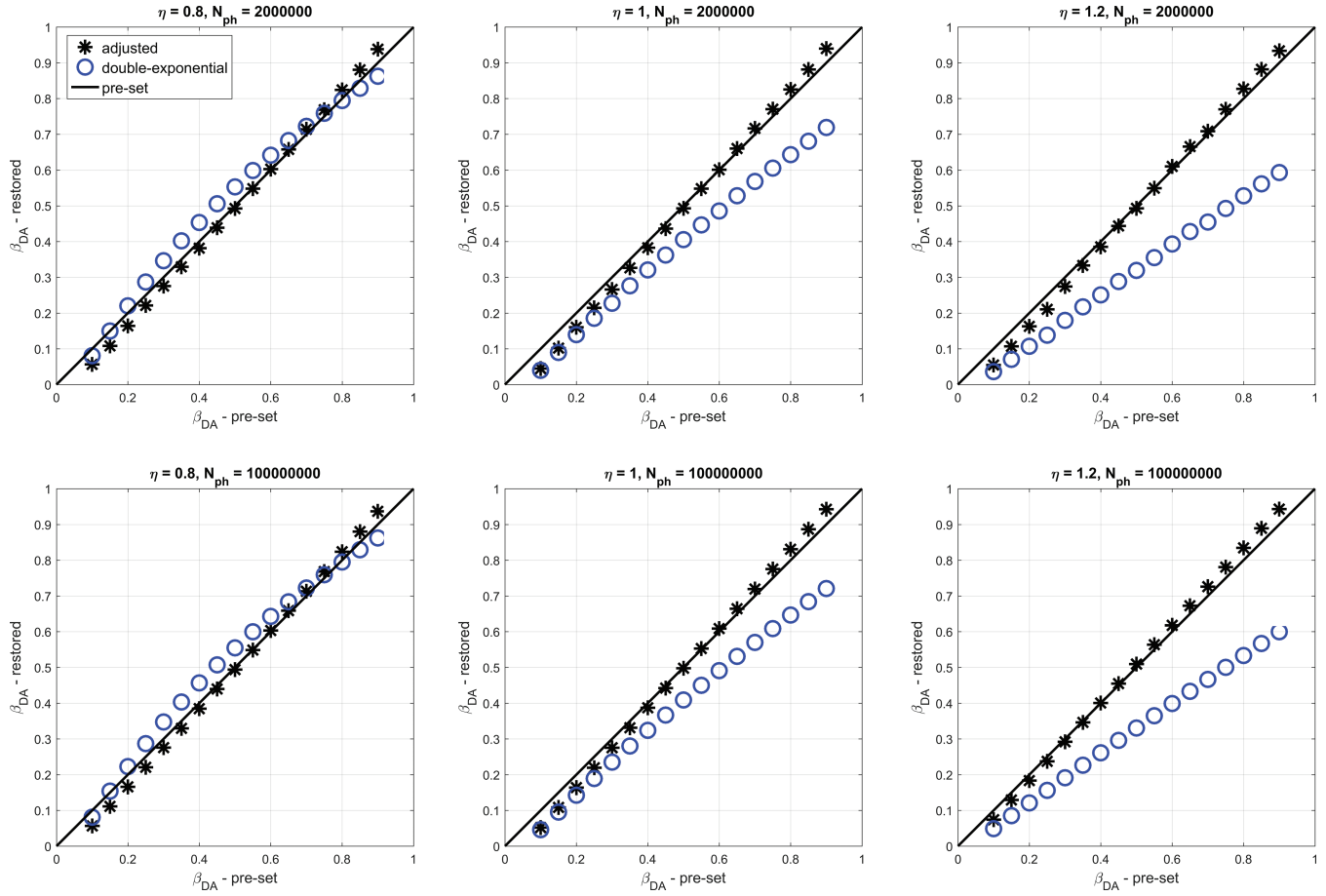

FIGURE 7 Molar fractions of FRETing molecules in the basic $s\kappa^2$ model preset (solid line), fitted by the 2-exp model (blue circles), and restored via the procedure using Eq. (4) (black stars)

by Eq. (20) and a simulated κ^2 PDDF obtained for randomly oriented donor-acceptor pairs is shown in Figure 5.

The simulated fluorescence decays presented in Figure 4 were carried out following the work of Berberan-Santos and Prieto [41]. As can be seen from Eq. (18), which is derived from Eq. (2.1) of reference [41], the probability $P_{ex}(t)$ that a donor remains in its excited state depends on the time-averaged history of the orientation factor κ^2 from 0 up to time t for that donor-acceptor pair, which is denoted $<\kappa^2>(t)$. As will be shown, as time elapses, $<\kappa^2>(t)$ tends to a constant value of 2/3, which is equal to that of the $d\kappa^2$ dynamic limit. By inspection of Eq. (18), it can be seen that the probability of a fluorophore being in its excited state at time t becomes a monoexponential function once sufficient time has elapsed that $<\kappa^2>(t)$ has time-averaged to a constant value. Therefore, once sufficient rotational randomization has occurred since excitation, the probability of the donor remaining in the excited state tends towards a monoexponential decay, which also corresponds to the fluorescence intensity decay tending towards being monoexponential. If the fluorescence decay time is short compared to the rotational motion, that is, $\tau_D < \min\{\tau_{rA}, \tau_{rD}\}$, then most of the fluorescence emission will occur before the decay becomes monoexponential. Conversely, if the fluorescence decay time is long compared to the

TABLE 1 Summary of the FRET parameters obtained from global fitting of the experimental data to a double exponential model (light grey columns) and the $s\kappa^2$ model (pale blue columns) adjusted to match the double exponential fit for the interactions of MST-1 with RASSF1-6

RASSF	Relative brightness	τ_D	τ_{DA} 2-exp	τ_{DA} $s\kappa^2$	E 2-exp	E $s\kappa^2$	η 2-exp	η $s\kappa^2$	β_{DA} 2-exp	β_{DA} $s\kappa^2$	K_D (mM) 2-exp	K_D (mM) $s\kappa^2$	K_D ratio
1	2.28	2632	889	1563	0.66	0.41	0.894	0.979	0.06	0.06	1.77	1.71	1.035
2	0.91	2682	1081	1736	0.60	0.35	0.937	1.031	0.08	0.09	0.43	0.37	1.162
3	0.75	2660	505	1192	0.81	0.55	0.785	0.848	0.14	0.10	0.84	1.16	0.724
4	0.69	2690	907	1597	0.66	0.41	0.893	0.979	0.09	0.09	0.41	0.39	1.051
5	0.82	2685	694	1400	0.74	0.48	0.839	0.913	0.075	0.07	0.65	0.75	0.867
6	0.55	2688	705	1412	0.73	0.47	0.842	0.916	0.1	0.09	0.31	0.35	0.885

Values calculated from the fit parameters are shown in dark grey and dark blue for the double exponential and $s\kappa^2$ models, respectively. The relative brightness of each RASSF-EGFP donor is also given, which was calculated from the time-integrated fluorescence intensity averaged over all the cells for that RASSF and then normalized to the average value obtained over all RASSFs for this experiment.

TABLE 2 Summary of the FRET parameters obtained from global fitting of the experimental data to a double exponential model (light grey columns) and the $s\kappa^2$ model (pale blue columns) adjusted to match the double exponential fit for the interactions of the SARAH domain construct with RASSF1-6

RASSF	Relative brightness	τ_D	τ_{DA} 2-exp	τ_{DA} $s\kappa^2$	E 2-exp	E $s\kappa^2$	η 2-exp	η $s\kappa^2$	β_{DA} 2-exp	β_{DA} $s\kappa^2$	K_D (mM) 2-exp	K_D (mM) $s\kappa^2$	K_D ratio
1	1.00	2632	781	1468	0.70	0.44	0.866	0.946	0.20	0.20	0.76	0.77	0.987
2	1.52	2682	956	1635	0.64	0.39	0.906	0.994	0.19	0.21	0.29	0.26	1.115
3	0.66	2660	716	1415	0.73	0.47	0.847	0.922	0.22	0.21	0.43	0.46	0.934
4	1.09	2690	865	1560	0.68	0.42	0.883	0.966	0.20	0.21	0.27	0.25	1.080
5	1.11	2685	805	1505	0.70	0.44	0.868	0.948	0.20	0.20	0.42	0.42	1.000
6	0.62	2688	688	1395	0.74	0.48	0.837	0.910	0.19	0.17	0.25	0.29	0.862

Values calculated from the fit parameters are shown in dark grey and dark blue for the double exponential and $s\kappa^2$ models, respectively. The relative brightness of each RASSF-EGFP donor is also given, which was calculated from the time-integrated fluorescence intensity averaged over all the cells for that RASSF and then normalized to the average value obtained over all RASSFs for this experiment.

rotational motion, that is, $\tau_D > \max\{\tau_{rA}, \tau_{rD}\}$, then the tail of the fluorescence decay will become monoexponential following an initial period of non-monoexponential decay. If $\tau_D >> \max\{\tau_{rA}, \tau_{rD}\}$, then the contribution of the initial non-monoexponential period to the total decay becomes negligible.

The transition between the monoexponential and non-monoexponential regimes can therefore be visualized by considering the temporal evolution of $<\kappa^2>(t)$. Figure 6 presents plots of distributions of this as a function of t^*, where, following [43], we define t^* as t scaled by the smaller of the donor and acceptor rotational correlation times, that is, $t^* = t/\min\{\tau_{rA}, \tau_{rD}\}$.

Figure 6 shows that for $q = 1$, corresponding to equal rotational correlation times of the donor and acceptor, the time-averaged distribution of $<\kappa^2>(t)$ approaches the $d\kappa^2$ dynamic limit of a constant value of 2/3 as time increases. Therefore, in the case of a random isotropic distribution of donor-acceptor orientations where the donor and acceptor have equal rotational correlation times, the observed decay profile of the time-dependent probability $P_{ex}(t)$ can be considered in two limits (see Eq. (18)). When t is much smaller than the rotational correlation time of the donor and acceptor, that is, $t^* << 1$, then $<\kappa^2>(t)$ will have the static random isotropic $s\kappa^2$ distribution, the decay will not be monoexponential and it will tend to that of the $s\kappa^2$ case. As $t^* \to \infty$, that is, t is much larger than the rotational correlation time of the donor and acceptor, $<\kappa^2>(t)$ will approach its time-averaged value of 2/3 and the decay will become monoexponential with the decay rate of the dynamic case.

In the case of $q = 0$ (ie, when one of the fluorophores is not rotating), as $t^* \to \infty$, then $<\kappa^2>(t)$ approaches a different limit as predicted by formula (2.33) in reference [41], namely $p_{s\kappa 2, q=0, t^*\to\infty}(\kappa^2) = \frac{1}{2\sqrt{\kappa^2 - 1/3}}$ in the range [1/3, 4/3] and 0 otherwise. Therefore, the fluorescence decay exhibits the $s\kappa^2$ decay profile for times $t^* << 1$ but exhibits a different (non-monoexponential) decay profile with a different distribution of decay rates as $t^* \to \infty$. Thus, this decay never becomes monoexponential. This can be explained by the observation that for each realization of a donor-acceptor pair, the orientation of the static fluorophore will produce a different limit for $<\kappa^2>(t)$ as $t^* \to \infty$.

3.3 | Correction of fluorescent protein FLIM FRET data fitted with $d\kappa^2$ model and evaluation of impact of fitting model on assays of protein binding kinetics in cells: RASSF-MST interaction

In our recent work, applying automated time-gated FLIM FRET microscopy to identify interaction partners and measure intracellular values of K_D for interactions between the RASSF and MST in cells [28], we based our analysis on the usual assumption of dynamic fluorophores with $\kappa^2 = 2/3$ and applied a conventional double exponential decay analysis method. Since the FRET measurements were made between enhanced green fluorescent protein (EGFP) and mCherry fluorescent protein (mCherryFP), some of the quantitative analysis could have been compromised by the "dynamic FRET" assumption—although the identification of RASSF1-6 as binding partners of MST binding is robust since it requires only detection of a significant reduction in donor lifetime due to FRET—and we note that the binding of MST1 to the RASSF proteins incorporating the Sav/RASSF/Hippo (SARAH) protein interaction domain (ie, RASSF1-6) was confirmed by biochemical measurements [42]. However, our estimates of the K_D values for these interactions were based on the values for the molar FRETing donor population fraction, β_{DA}, determined by the fitting of FLIM FRET data globally to a double exponential ($d\kappa^2$) model. Accordingly, we were interested to explore the potential impact of FLIM FRET analysis based on the $s\kappa^2$ model, since this represents a more realistic description of these FRET measurements utilizing fluorescent protein constructs.

Because our nonlinear fluorescence decay fitting software tool incorporating the $s\kappa^2$ model of Eq. (15) is not yet able to be applied to image data, we developed a method to "correct" our existing RASSF-MST1 FLIM FRET data, which was obtained by global fitting of a double exponential decay model to the experimental data using *FLIMfit*. First, we generated a noise-free double exponential donor

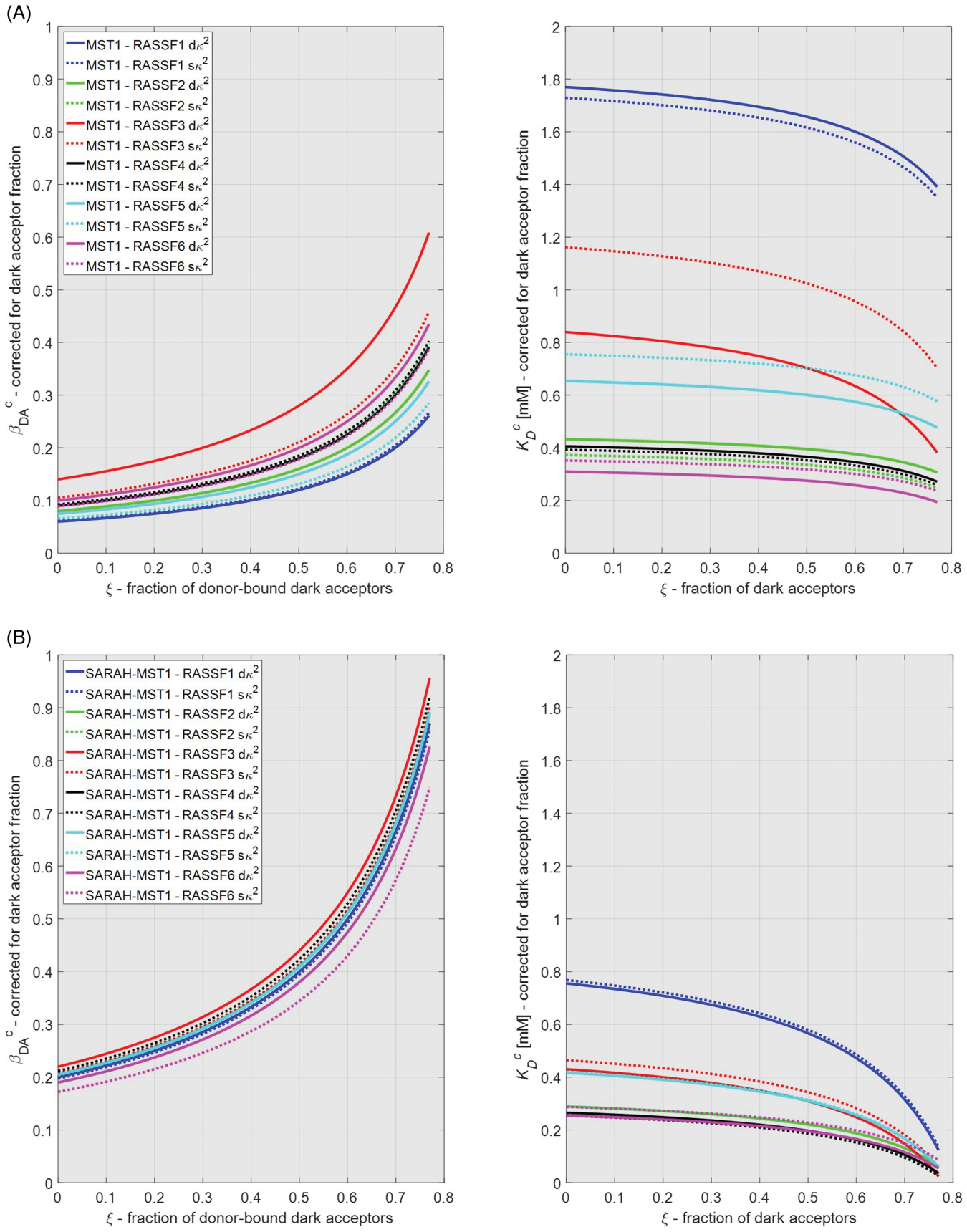

FIGURE 8 Variation of the corrected fraction of bound donors, β_{DA}^{c}, and corresponding K_D^c values for the RASSF/MST1 FLIM FRET data as a function of the fraction of dark acceptors, ξ: A, RASSF1-6 interacting with full length MST1. B, RASSF1-6 interacting with truncated SARAH domain

fluorescence decay profile for each RASSF-MST1 family member interaction using the FRET parameters obtained from the fitting of the experimental data. We then adjusted a simulated $s\kappa^2$ fluorescence decay profile to fit these ideal double exponential donor fluorescence decay profiles. Thus, we obtained the $s\kappa^2$ model-based FRET parameters for each RASSF-MST1 family member interaction. For this fitting procedure, the non-FRETing donor lifetime of the simulated $s\kappa^2$ decay was fixed to the mean value of a single exponential fit of the EGFP fluorescence in cells expressing only the donor fluorophore, and the $s\kappa^2$ model parameters $\eta_{\mathrm{DA},s\kappa^2}$ and $\beta_{\mathrm{DA},s\kappa^2}$ were adjusted using a multidimensional nonlinear minimization (Nelder-Mead) [43] fit to match the double exponential decay profile. Thus, the following function was minimized to fit the $s\kappa^2$ model to the "ideal" experimentally derived double exponential decay profiles:

$$\left[\eta_{s\kappa^2},\beta_{\mathrm{DA},s\kappa^2}\right]=\operatorname{argmin}\left\{\sum_{t=0}^{\infty}\left[f_{d\kappa^2}\left(\beta_{\mathrm{DA},d\kappa^2},\tau_{D,d\kappa^2},\tau_{\mathrm{DA},d\kappa^2},t\right)-f_{s\kappa^2}\left(\beta_{\mathrm{DA},s\kappa^2},\tau_{D,d\kappa^2},\eta_{s\kappa^2},t\right)\right]^2\right\}, \tag{4}$$

where $f_{d\kappa^2}$ and $f_{s\kappa^2}$ are double exponential and $s\kappa^2$ fluorescence decays respectively.

In order to validate this approach, we simulated $s\kappa^2$ decay curves using the same parameters used above, that is, $\eta = \{0.8,\ 1,\ 1.2\}$, $N_{\mathrm{ph}} = \{2{\cdot}10^6,\ 10^8\}$ and $\beta_{\mathrm{DA}} = 0.05$ to 0.95. We then fitted these decay profiles to the standard double exponential decay model that is widely used for FLIM data analysis. The simulations and the global double exponential fits were performed the same way as described in Section 3.1. We then applied the correction approach of Eq. (4) to restore the original parameters of the $s\kappa^2$ decays using only the results of the double exponential fits. The results of this procedure are shown in Figure 7.

One can see that the correction based on Eq. (4) provides an improvement in the molar fraction values, especially for the cases of weaker FRET (larger η). This improvement does not seem to be highly sensitive to the number of photons in the decay. The corresponding plots for the donor/acceptor spatial separation parameter, η, showed very good agreement between original vs restored values (within 2% everywhere; data not shown).

We then applied this correction procedure to our previously published FLIM FRET data for RASSF-MST interactions [28] that had previously been fitted using a double exponential decay model. The results of this $s\kappa^2$ correction procedure are summarized in Tables 1 and 2, which present the median values of intracellular K_{D} measured per cell reported in [28], the values of K_{D} obtained from the $s\kappa^2$ fluorescence decay adjusted to match the double exponential decay curve fitted to the experimental data and the relative change in K_{D} between the two models. As discussed in [28], the dissociation constant, K_{D}, is related to the FRETing population fraction, β_{DA}, by:

$$K_{\mathrm{D}}=\frac{(1-\beta_{\mathrm{DA}})(1-(\beta_{\mathrm{DA}}D_{\mathrm{total}}/A_{\mathrm{total}}))A_{\mathrm{total}}}{\beta_{\mathrm{DA}}}, \tag{5}$$

where D_{total} and A_{total} are the total concentrations of donor and acceptor fluorophores that can be determined via calibrated fluorescence intensity measurements.

It is apparent that the values of β_{DA} and K_{D} found for the MST1-RASSF1-6 and SARAH-RASSF1-6 interactions via double exponential FRET analysis deviate from those obtained using the $s\kappa^2$ model within a factor of <1.4.

We note that this approach could be used generally to apply an $s\kappa^2$ model "correction" to any FRET experiments for which the conventionally calculated FRET parameters can be used to describe a donor fluorescence decay curve. This could be useful where FRET constructs have been employed such that the assumption of a static random distribution of fluorescent protein dipole orientations would provide more accurate FRET parameters, as is the case for fluorescent protein-based constructs.

As well as the impact of fluorophores that are effectively static during the donor fluorescence decay, quantitative FLIM FRET measurements using fluorescent proteins can also be compromised by the presence of "dark" acceptors that lead to donor-acceptor complexes not being accounted for in the FRETing population fraction, which can also lead to errors when calculating K_{D}. Dark acceptor states have previously been reported for the red fluorescent protein mCherryFP [44, 45] and this could be a source of error when determining the bound molar fraction of RASSF proteins. The presence of dark acceptors will result in the measured values of β_{DA} and A_{total} being reduced from their true values by $(1-\xi)$, where ξ is the fraction of acceptors in the dark state. This effect may be corrected post-fitting of the FLIM data by appropriately rescaling the fitted values of β_{DA} and the measured value of A_{total}. The corrected molar fraction of donors bound to all acceptors (both bright and dark) can be calculated as:

$$\beta_{\mathrm{DA}}^{\mathrm{c}}=\frac{\beta_{\mathrm{DA}}}{1-\xi}. \tag{6}$$

Thus, the corrected expression for K_{D} becomes, correspondingly:

$$K_{\mathrm{D}}^{\mathrm{c}}=\frac{(1-(\beta_{\mathrm{DA}}/(1-\xi)))(1-(\beta_{\mathrm{DA}}D_{\mathrm{total}}/A_{\mathrm{total}}))A_{\mathrm{total}}}{\beta_{\mathrm{DA}}}. \tag{7}$$

This derivation assumes that donors bound to dark acceptors have the same fluorescence decay profile as unbound donors. The constraint that the total number of acceptors bound to donors cannot exceed the number of available donors yields the condition $\beta_{\mathrm{DA}} \le 1-\xi$, which

limits the applicability of Eqs. (6) and (7) to the range of physically possible cases.

Figure 8 illustrates how the presence of dark acceptor states could impact the analysis of the RASSF/MST1 FLIM FRET data, plotted with the values of β_{DA}^{c} and K_D^c calculated for the case of dynamic and static random isotropic distributions of fluorophores for RASSF1-6. For values of ξ up to ~0.5, the impact of dark acceptors on measurements of K_D is relatively small (changing K_D values by a factor of less than ~1.4) and comparable to the small difference in K_D values for the double exponential and $s\kappa^2$ models found for this case.

4 | METHODS

4.1 | The $s\kappa^2$ intensity decay model

In the following derivation, $P_T(t)$ represents the PDDF of photons detected within the measurement window $[0,T]$ resulting from a fluorescence decay profile exited by an infinitely short laser pulse at time $t = 0$.

For example, for a monoexponential fluorescence decay with the lifetime τ, this probability is [20, 46]

$$P_{T\_1\exp}(t) = \frac{1}{\tau}\cdot\frac{1}{1-e^{-T/\tau}}e^{-t/\tau}, \tag{8}$$

where the factor $(1/(1 - e^{-T/\tau}))$ in Eq. (8) takes into account the effect of incomplete exponential decays [46].

In general, the fluorescence intensity, $I_T(t)$, experimentally observed over each pulse period T is given by the photon arrival probability, $P_T(t)$, convolved with the instrument response function, IRF(t), multiplied by N_{ph}, the total number of photons in the total decay:

$$I_T(t) = N_{ph}\cdot P_T(t)\otimes \mathrm{IRF}(t). \tag{9}$$

The function IRF(t) is the PDDF of photon arrival delays in the window $[0,T]$ due to the measurement instrumentation only. It may be considered as the response of the measurement system to a sample with an infinitely fast decay profile.

The conventional double exponential FRET model for a mixture of free donor and donor-acceptor (FRET) molecular states can be derived from Eq. (8) as a weighted sum of the donor and the donor-acceptor exponential terms parameterized by their respective lifetimes τ_D and τ_{DA}, that is

$$P_{T\_\mathrm{FRET},2\exp}(t) = f_D\cdot P_{T\_1\exp}(t,\tau_D) + (1-f_D)\cdot P_{T\_1\exp}(t,\tau_{DA}), \tag{10}$$

where f_D is the fraction of photons emitted by non-FRETing donor fluorophores. In this case, τ_D and τ_{DA} are related by the FRET efficiency as follows:

$$\tau_{DA} = \tau_D(1-E). \tag{11}$$

If the FRET efficiency is distributed with probability density $p_{FRET}(E)$, the photon arrival probability becomes:

$$\begin{aligned} P_{T\_\mathrm{FRET}}(t;\tau_D,\ldots) &= f_D\cdot P_{T\_1\exp}(t,\tau_D) \\ &+ (1-f_D)\cdot\int_E P_{T\_1\exp}(t,\tau_D(1-E))\cdot p_{\mathrm{FRET}}(E)dE. \end{aligned} \tag{12}$$

In general, the probability distribution function $p_{FRET}(E)$ entering Eq. (12) depends on the donor/acceptor geometry. In particular, the case of a "static random isotropic orientation" of the orientation factor κ^2 of the donor and acceptor dipoles (ie, the $s\kappa^2$ model mentioned above) is described by the analytical κ^2 distribution first published in [41]; the corresponding FRET efficiency distribution was derived in [3]. For a given donor/acceptor pair, it can be assumed that this distribution $p_{\mathrm{FRET}\,s\kappa^2}(E)$ depends only on the parameter η, which is the dimensionless donor-to-acceptor distance as defined in Eq. (1). Namely, for the given parameters η and E, this probability distribution is calculated as follows:

$$p_{\mathrm{FRET}\,s\kappa^2}(E,\eta) = \begin{cases} H\cdot\ln\left(2+\sqrt{3}\right), & 0 \le E \le \dfrac{F}{1+F}, \\ H\cdot\ln\left(\dfrac{2+\sqrt{3}}{G+\sqrt{G^2-1}}\right), & \dfrac{F}{1+F} \le E \le \dfrac{4F}{1+4F}, \\ 0, & \dfrac{4F}{1+4F} \le E \le 1, \end{cases} \tag{13}$$

$$\text{where } F = \frac{3}{2\eta^6};\quad G = \sqrt{\frac{E}{F(1-E)}};\quad H = \frac{1}{2(1-E)\sqrt{3EF(1-E)}}. \tag{14}$$

For numerical calculations, a discrete approximation of the integral in Eq. (12) is made using the set of FRET efficiency probabilities: $p(E) \Rightarrow p(E_k)$, where E_k are 1000 equidistant values between 0 and 1 (excluding these extreme values).

An expression for the $s\kappa^2$ intensity decay model is then obtained by combining Eq. (12) with the discrete approximation of $p_{\mathrm{FRET}\,s\kappa^2}(E)$ and substituting into Eq. (9):

$$\begin{aligned} &I_{T\_\mathrm{FRET}\_s\kappa^2}(t;\tau_D,\eta,f_D) \\ &= N_{ph}\left(f_D\cdot P_{T\_1\exp}(t,\tau_D) + (1-f_D)P_{T\_s\kappa 2}(t;\tau_D,\eta)\right)\otimes\mathrm{IRF}(t), \\ &P_{T\_s\kappa^2}(t;\tau_D,\eta) = \sum_k p_{\mathrm{FRET}\,s\kappa^2}(E_k,\eta)\cdot P_{T\_1\exp}(t,\tau_D(1-E_k)). \end{aligned} \tag{15}$$

4.2 | Simulated $s\kappa^2$ FRET data generation

The $s\kappa^2$ fluorescence decay model was coded in MATLAB using Eq. (15). To simulate typical experimental fluorescence decay profiles, a decay consisting of 4096 time bins with a 20 MHz laser pulse repetition rate was simulated, as is typical for time-correlated single photon counting (TCSPC) measurements. An experimentally measured IRF was used in the simulations and Poisson noise was added to the modelled decay after convolving it with the IRF.

4.3 | Fitting to the $s\kappa^2$ and $d\kappa^2$ models

From a coding perspective, nonlinear fitting of a fluorescence decay to the $s\kappa^2$ model of Eq. (15) involves 3 fitting parameters, τ_D, η and f_D. For a specific fit, the first 2 parameters define the probability distribution, $p_{\mathrm{FRET}\,s\kappa^2}(E_k)$, used to generate the fitting model. Once the fitting process has yielded a given τ_D, η and f_D, the FRET efficiency, $\langle E\rangle = \sum_k p_{\mathrm{FRET}\,s\kappa^2}(E_k)E_k$, and the average FRETing donor lifetime, $\tau_{DA} = \tau_D(1 - \langle E\rangle)$, can be obtained, and then the population (molar) fractions of free donor and donor-acceptor states, β_D and β_{DA}, can be calculated [21]. For example, for the FRETing molar fraction β_{DA}, one obtains:

$$\beta_{DA} = \frac{f_{DA}\tau_{DA}{}^{-1}}{f_{DA}\tau_{DA}{}^{-1} + f_D\tau_D{}^{-1}}, \text{ where } f_{DA} = (1 - f_D). \quad (16)$$

4.4 | Global fitting to the $s\kappa^2$ and $d\kappa^2$ models

To globally fit the fluorescence lifetime decays to the $s\kappa^2$ and $d\kappa^2$ models, the global versions of Eqs. (10) and (15) were derived and the well-known variable projection method separating linear and nonlinear variables [30] was applied. For example, the model described by Eq. (15) was modified as:

$$I_{\mathrm{FRET\_}sk^2}(t) = \left(c_D \cdot P_{T\_1}\exp(t,\tau_D) + c_{\mathrm{FRET}}P_{T\_s\kappa^2}(t;\tau_D,\eta)\right)\otimes \mathrm{IRF}(t), \quad (17)$$

where c_D, c_{FRET} are the linear fitted amplitudes, and other variables are the same as in Eq. (15). In this case, the nonlinear (global) parameters of the fit are τ_D and $\eta = R_{DA}/R_0$. Global fitting to the $s\kappa^2$ and $d\kappa^2$ models was then undertaken using the MATLAB implementation of the "varpro" procedure [31]. For both models, the components' photon decay fractions f_D and f_{DA} are calculated from the linear amplitudes. For example, the donor fraction is $f_D = c_D/(c_D + c_{\mathrm{FRET}})$, and the corresponding FRET fraction is complementary.

4.5 | Simulations of fluorescence intensity decays for varying rotational mobility of fluorophores

In order to get an insight into the interplay of static and dynamic regimes in FRET, we utilized the rotational diffusion simulation recipes presented in the article by Berberan-Santos et al. [41].

The basis for decay simulation is the time-dependent probability $P_{ex}(t)$ of the donor in a molecular FRET pair to stay excited at time t after the excitation at $t = 0$ [34–41], which in the notation used here is

$$P_{ex}(t) = \exp\left(-\frac{t}{\tau_D}\left[1 + \frac{3}{2}\eta^{-6}\cdot <\kappa^2>(t)\right]\right), \quad (18)$$

where the time-dependent function of interest $<\kappa^2>(t)$ is the orientation factor time-averaged from times 0 to t:

$$<\kappa^2>(t) = \frac{1}{t}\int_0^t \kappa^2(t')dt'.$$

Note that substituting 2/3 instead of the function of interest $<\kappa^2>(t)$ in Eq. (18) gives the well-known dynamic FRET decay. When mixed with a non-FRETing donor term, it produces the $d\kappa^2$ model.

In reference [41], simulations of intermediate regimes included the effect of different rotational properties of donor and acceptor, which leads to a refined model:

$$P_{\mathrm{ex\,sim}}(t) = \exp\left(-\frac{t}{\tau_D}\left[1 + \frac{3}{2}\eta^{-6}\cdot <\kappa^2>_q(t^*)\right]\right). \quad (19)$$

In Eq. (19), the t-dependent term $<\kappa^2>_q(t^*)$ was obtained through numerical simulation. This term depends on the parameter q, which is the ratio of the smaller of the donor or acceptor rotational correlation time to the larger of the donor or acceptor rotational correlation time. At $q = 0$ either the donor or acceptor is static, whereas at $q = 1$ both have the same rotational correlation time. Numerical simulations were performed as a function of the dimensionless time $t^* = t/\tau_r$, where τ_r is the smaller rotational correlation time (either of donor or acceptor) [41].

To calculate a macroscopically averaged emission probability, $P_{\mathrm{ex\ m}}(t)$, and the evolution of $<\kappa^2>_q(t^*)$ over time, we simulated 60 000 realizations of the orientation of donor-acceptor pairs as a function of time. To calculate PDDFs of $<\kappa^2>_q(t^*)$ shown in Figure 6, the scaled simulated orientation $\kappa^2{}_q(t^*)$ factors were integrated numerically over time and a normalized histogram was constructed. To calculate a simulated decay, for each pair the simulated orientation factors $\kappa^2{}_q(t^*)$ were scaled appropriately onto an "instrument" time axis, depending on the values of τ_r and the value of q to yield $\kappa^2{}_q(t)$ for that pair. $P_{\mathrm{ex\ m}}(t)$ was then estimated as the average of the decay (Eq. (19)) over all realizations: $P_{\mathrm{ex\ m}}(t) \approx <P_{\mathrm{ex\ sim}}(t)>_{\mathrm{realizations}}$. Having obtained the macroscopic probability $P_{\mathrm{ex\ m}}(t)$, the intensity of fluorescence decay (which is measured by FRET and FLIM/FRET instruments in photons/s) could then be calculated as $I(t) = N_{\mathrm{ph}}\left(-\frac{dP_{exm}(t)}{dt}\right)$. These are the decays plotted in Figure 4.

Figure 9 illustrates the evolution of exemplar simulated $\langle\kappa^2\rangle_q(t^*)$ curves for $q = 0$, 0.5 and 1, that have been interpolated onto the t axis in the "instrument window" for three different values of τ_r.

4.6 | Calculation of κ^2 distribution for static donor-acceptor fluorophores and corresponding decay curves

The theoretical κ^2 distribution shown in Figure 5 was obtained using the formula given in [41]:

$$p_{s\kappa^2}(\kappa^2) = \frac{1}{2\sqrt{3\kappa^2}}\left[\ln\left(2+\sqrt{3}\right) - \theta(\kappa^2-1)\ln\left(\sqrt{\kappa^2}+\sqrt{\kappa^2-1}\right)\right], \quad (20)$$

where θ is the Heaviside function.

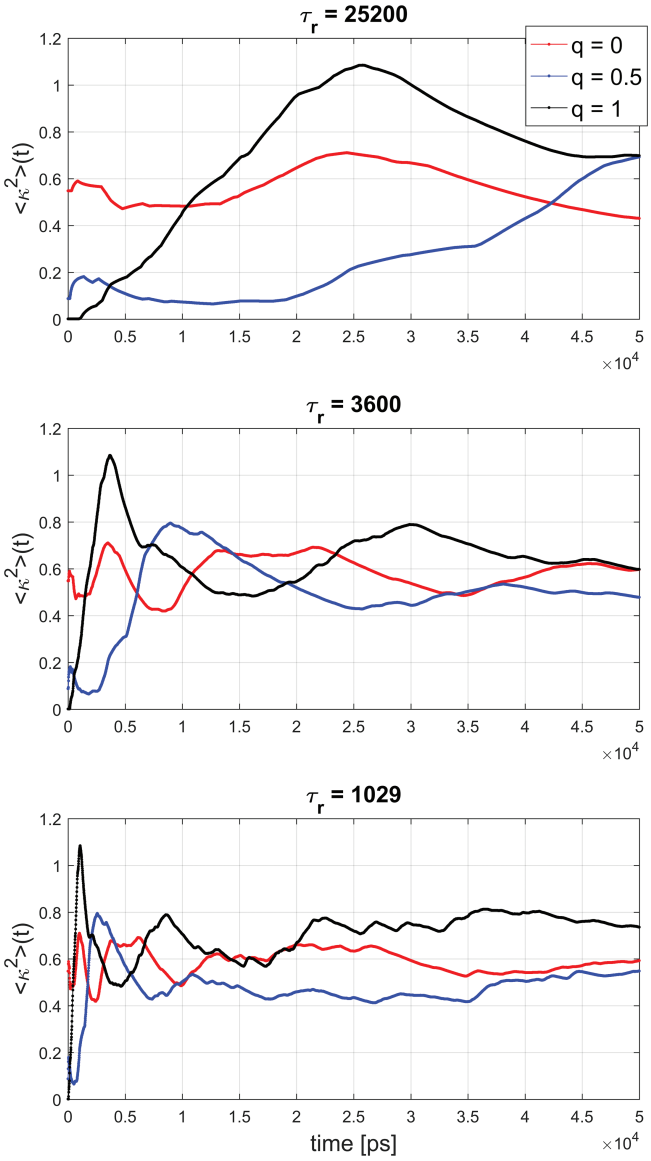

FIGURE 9 The same three simulated functions $\langle\kappa^2_q\rangle(t^*)$ are interpolated on different scales to produce $\langle\kappa^2_q\rangle(t)$ functions for three different values of τ_r

The simulated κ^2 distribution shown in Figure 5 was obtained through numerical simulation of randomly oriented donor-acceptor pairs.

To simulate the $s\kappa^2$ fluorescence intensity decay in Figure 4, we used Eq. (18) and employed the PDDF of Eq. (20) in the place of $<\kappa^2>(t)$. The resulting curve coincides with the one obtained from the $p_{\mathrm{FRET}\,s\kappa^2}(E)$ PDDF given in Eq. (13)) (magenta curve) and so is not shown in Figure 4.

4.7 | FLIM FRET measurements of MST1-RASSF interactions

The details of the experiment reported in reference [28] are summarized here. Briefly, we utilized wide-field time-gated imaging to realize a FLIM microscope that is able to automatically acquire optically sectioned fluorescence lifetime images with a typical mean acquisition time of 10 seconds. To obtain reliable statistics, the FLIM images were acquired from 10 FOV per well, using 5 time gates to sample the fluorescence decay profiles with exposure times around 1 second per gate for the donor (EGFP) images. The images were automatically segmented using the *FLIMfit* cell segmentation tools and decays were fitted on a per-cell basis using a global double exponential analysis where the long (donor only) decay component was fixed to the value obtained from cells expressing only the donor.

5 | CONCLUSIONS

FRET measurements are widely used to study molecular processes, particularly in cell biology using fluorescent proteins. Unfortunately, almost all previous work assumes the dynamic random distribution of fluorophore orientations, that is, that the FRETing donor can be described by a monoexponential fluorescence decay profile, which is not appropriate for FRET with fluorescent proteins. As pointed out by Vogel et al. [3], the static random distribution of fluorophore orientations leads to a bimodal FRET efficiency distribution that does not produce a monoexponential fluorescence decay. The static random distribution of fluorophore orientations is thought to be a better model for the donor decay for FRET with fluorescent proteins. Many researchers have used fluorescence lifetime measurements of FRET with fluorescent proteins to quantitate cell-signalling processes, including our recent intracellular measurements of the dissociation constants K_D, of molecular interactions, and so it is important to understand the applicability and the impact of the static $s\kappa^2$ random distribution of fluorescent protein dipole orientations on such quantitative FRET analyses.

Here, we have followed [3] to develop a numerical simulation of $s\kappa^2$ fluorophore emission and have studied its impact on the quantification of FRETing donor population fraction for the first time, with a view to estimating its effect on measurements of K_D. We have also developed and evaluated an algorithm for the $s\kappa^2$ model-based nonlinear fitting of FRETing donor fluorescence decay profiles. We observe that the discrepancy between the FRET parameters obtained for the dynamic and static FRET models varies as a function of the donor-acceptor distance. Our simulations show that global fitting provides the most robust analysis, which we believe to be due to the reduction in the number of fit parameters used with global fitting. In general, it was found that the fit of simulated $s\kappa^2$ FRET lifetime data to a double exponential decay model tended to result in an overestimate of the effective FRET efficiency and often also the donor molar fraction.

To support further analysis of the static $s\kappa^2$ distribution of fluorescent protein dipole orientations, we compared simulated fluorescence decay profiles to decay profiles generated using the analytic expression for the FRET efficiency distribution of [3] (Eq. (13)) and to decay profiles generated

using the analytic static κ^2 distribution given in [41] (Eq. (20)). Good agreement was found between our simulations and the two theoretical methods. Our simulations allowed us to explore the transition between the static $s\kappa^2$ and dynamic $d\kappa^2$ limits of FRETing fluorophores as the ratio of the rotational correlation time of the donor/acceptor to the fluorescence decay time is varied and also to explore the use of donor/acceptor pairs with different rotational correlation times.

We have also studied the impact of the static $s\kappa^2$ random distribution of fluorescent protein dipole orientations on our previously published FLIM FRET data [28] concerning the interactions of RASSF family proteins with MST1 and its truncated SARAH domain, which included calculations of K_D. By fitting the $s\kappa^2$ model to ideal double exponential decay profiles incorporating the FRET parameters obtained from our global fitting of the experimental fluorescence decays for each FRET experiment, we were able to obtain estimates of the relevant FRET parameters corresponding to the $s\kappa^2$ interpretation. Our analysis indicates that, while the β_{DA} values calculated with assumption of the double exponential decay model may incorrectly estimate the K_D values corresponding to the static fluorescence protein donor emission, the discrepancy was less than a factor of 1.4 in this case, as expected for the relatively low FRET efficiencies and FRETing population fractions. However, the approach demonstrated can provide values that are more accurate—compared to fitting data to a double exponential decay—and could be generally applied to improve FRET measurements using fluorescence proteins or other fluorescently labelled protein moieties that are effectively static over the timescale of the fluorescent decay. In future, we hope to integrate the $s\kappa^2$ data model into our FLIM data analysis software.

Finally, we suggest that the methodology presented can be more broadly applied to analyse complex FRET signals arising from a range of FRET efficiency distributions (appropriately modifying Eq. (15)). We note that similar routine FRET fitting techniques based on the direct "on the fly" modelling were investigated before, for example, [35]. In future, it would be interesting to study the impact of donor/acceptor distance distributions and modification of the $s\kappa^2$ model to include some constraints on the range of donor/acceptor static orientation angles.

Our MATLAB software to apply the "$s\kappa^2$ correction" to FLIM FRET data of measurements made with fluorescent proteins can be found at https://github.com/yalexand/dk2_to_sk2_calculator.

ACKNOWLEDGMENTS

The authors thank Sean Warren for valuable discussions, including a correction to the implementation of global fitting method used here. The authors gratefully acknowledge funding from the UK Medical Research Council (MRC, MR/K015834/1) and the Biotechnology and Biological Sciences Research Council (BBSRC, BB/M006786/1).

REFERENCES

[1] T. Förster, *Fluoreszenz Organischer Verbindungen*, Vandenhoeck & Ruprecht, Göttingen **1951**.
[2] J. R. Lakowicz, *Principles of Fluorescence Spectroscopy*, 2nd ed., Kluwer Academic, New York, NY **1999**, p. 369.
[3] S. S. Vogel, T. A. Nguyen, B. W. van der Meer, P. S. Blank, *PLoS One* **2012**, *7*, e49593.
[4] F. Ciruela, *Curr. Opin. Biotechnol.* **2008**, *19*, 338.
[5] K. Aoki, E. Kiyokawa, T. Nakamura, M. Matsuda, *Phil. Trans. R. Soc. B* **2008**, *363*, 2143.
[6] C. M. Welch, H. Elliott, G. Danuser, K. M. Hahn, *Nat. Rev. Mol. Cell Biol.* **2011**, *12*, 749.
[7] A. Nezu, A. Tanimura, T. Morita, A. Shitara, Y. Tojyo, *BBA Gen. Subjects* **2006**, *1760*, 1274.
[8] T. Nishioka, K. Aoki, K. Hikake, H. Yoshizaki, E. Kiyokawa, M. Matsuda, *Mol. Biol. Cell* **2008**, *19*, 4213.
[9] D. Stockholm, M. Bartoli, G. Sillon, N. Bourg, J. Davoust, I. Richard, *J. Mol. Biol.* **2005**, *346*, 215.
[10] K. M. Dean, T. Qin, A. Palmer, *Biochim. Biophys. Acta* **1823**, *2102*, 1406.
[11] A. Miyawaki, J. Llopis, R. Heim, J. M. McCaffery, J. A. Adams, M. Ikura, R. Y. Tsien, *Nature* **1997**, *388*, 882.
[12] M. Mank, D. F. Reiff, N. Heim, M. W. Friedrich, A. Borst, O. Griesbeck, *Biophys. J.* **2006**, *90*, 1790.
[13] H. Ueyama, M. Takagi, S. Takenaka, *J. Am. Chem. Soc.* **2002**, *124*, 14286.
[14] T. Kuner, G. J. Augustine, *Neuron* **2000**, *27*, 447.
[15] E. A. Jares-Erijman, T. M. Jovin, *Curr. Opin. Chem. Biol.* **2006**, *10*, 409.
[16] T. W. J. Gadella Ed., *FRET and FLIM Techniques, Volume 33 in Laboratory Techniques in Biochemistry and Molecular Biology*, Elsevier Science, Amsterdam, Oxford, 2008, ISBN:9780080915128
[17] S. S. Vogel, C. Thaler, S. V. Koushik, *Sci. STKE* **2006**, *2006*(331), re2.
[18] A. Hoppe, K. Christensen, J. A. Swanson, *Biophys. J.* **2002**, *83*, 3652.
[19] J. R. Lakowicz, *Principles of Fluorescence Spectroscopy*, 2nd ed., Vol. 129, Kluwer Academic, New York, NY **1999**, p. 98.
[20] K. Walther, B. Papke, M. B. Sinn, K. Michel, A. Kinkhabwala, *Mol. BioSyst.* **2011**, *7*, 322.
[21] E. Barnoy, R. Popovtzer, D. Fixler, *J. Biophotonics* **2018**, *11*, e201700084.
[22] M. Köllner, J. Wolfrum, *Chem. Phys. Lett.* **1992**, *200*, 199.
[23] A. H. A. Clayton, Q. S. Hanley, P. J. Verveer, *J. Microsc.* **2004**, *213*, 1.
[24] M. A. Digman, V. R. Caiolfa, M. Zamai, E. Gratton, *Biophys. J.* **2008**, *94*, L14.
[25] S. Pelet, M. J. R. Previte, L. H. Laiho, P. T. C. So, *Biophys. J.* **2004**, *87*, 2807.
[26] H. E. Grecco, P. Roda-Navarro, A. Girod, J. Hou, T. Frahm, D. C. Truxius, R. Pepperkok, A. Squire, P. I. Bastiaens, *Nat. Methods* **2010**, *7*, 467.
[27] D. Alibhai, D. Kelly, S. Warren, S. Kumar, A. Margineau, R. Serwa, E. Thinon, Y. Alexandrov, E. Murray, F. Stuhmeier, E. Tate, M. Neil, C. Dunsby, P. M. W. French, *J. Biophotonics* **2013**, *6*, 398.
[28] A. Margineanu, J. J. Chan, D. J. Kelly, S. C. Warren, D. Flatters, S. Kumar, M. Katan, C. W. Dunsby, P. M. W. French, *Sci. Rep.* **2016**, *6*, 28186.
[29] S. C. Warren, A. Margineanu, D. Alibhai, D. J. Kelly, C. Talbot, Y. Alexandrov, I. Munro, M. Katan, C. Dunsby, P. M. W. French, *PLoS One* **2013**, *8*, e70687.
[30] G. Golub, V. Pereyra, *Inverse Probl.* **2003**, *19*, R1.
[31] D. O'Leary, B. Rust, *Comput. Optim. Appl.* **2013**, *54*, 579.
[32] R. M. Dickson, A. B. Cubitt, R. Y. Tsien, W. E. Moerner, *Nature* **1997**, *388*, 355.
[33] J. Hendrix, C. Flors, P. Dedecker, J. Hofkens, Y. Engelborghs, *Biophys. J.* **2008**, *94*, 4103.
[34] R. E. Dale, J. Eisinger, W. E. Blumberg, *Biophys. J.* **1979**, *26*, 161.
[35] P. Wu, L. Brand, *Biochemistry* **1992**, *31*, 7939.
[36] B. W. van der Meer, *Rev. Mol. Biotechnol.* **2002**, *82*, 181.
[37] E. Pham, J. Chiang, I. Li, W. Shum, K. Truong, *Structure* **2007**, *15*, 515.
[38] E. Deplazes, D. Jayatilaka, B. Corry, *Phys. Chem. Chem. Phys.* **2011**, *13*, 11045.

[39] S. Vogel, B. W. van der Meer, P. S. Blank, *Methods* **2013**, *66*, 131.
[40] R. E. Dale, *Acta Phys. Pol.* **1978**, *A54*, 743.
[41] M. N. Berberan-Santos, M. J. E. Prieto, *J. Chem. Phys.* **1988**, *88*, 6341.
[42] J. J. Chan, D. Flatters, F. Rodriguez-Lima, J. Yan, K. Thalassinos, M. Katan, *Adv. Biol. Regul.* **2013**, *53*, 190.
[43] MATLAB "fminsearch" function, https://mathworks.com/help/matlab/ref/fminsearch.html
[44] L. Hillesheim, Y. Chen, J. Muller, *Biophys. J.* **2006**, *91*, 4273.
[45] S. Padilla-Parra, N. Auduge, H. Lalucque, J.-C. Mevel, M. Coppey-Moisan, M. Tramier, *Biophys. J.* **2009**, *97*, 2368.
[46] P. R. Barber, S. M. Ameer-Beg, J. D. Gilbey, R. J. Edens, I. Ezike, B. Vojnovic, *Proc. SPIE* **2005**, *5700*, 171.

How to cite this article: Alexandrov Y, Nikolic DS, Dunsby C, French PMW. Quantitative time domain analysis of lifetime-based Förster resonant energy transfer measurements with fluorescent proteins: Static random isotropic fluorophore orientation distributions. *J. Biophotonics*. 2018;11:e201700366. https://doi.org/10.1002/jbio.201700366